Dielectric Cover Effect on Rectangular Microstrip Antenna Array

Reuven Shavit

Abstract—**A theoretical model to analyze a covered rectangular antenna with an arbitrary dielectric constant superstrate is developed. The antenna is simulated by the radiation of two magnetic dipoles located at the radiating edges of the patch. The Green's function of an elementary magnetic dipole in a superstrate–substrate structure, utilizing spectral-domain analysis, is formulated, and the surface-wave and radiation field are computed. An improved transmission line model, which considers the stored energy near the radiating edges and the external mutual coupling, is used to compute the input impedances and radiation efficiency. Design considerations on the superstrate thickness and its dielectric constant are discussed. Experimental data for a single element and a 4×4 microstrip array is presented to validate the theory.**

I. Introduction

The increasing use of microstrip antennas in the electronic communication market requires simple models to analyze their performance. The transmission line model [1] is one of the simplest of the somewhat successful models for analyzing uncovered rectangular microstrip antennas. This paper attempts to implement the same concepts to the analysis of a rectangular microstrip antenna covered with a dielectric superstrate layer. In many applications a radome to protect the antenna is required. The dielectric cover offers such a protection and keeps the antenna low profile. However, it has impedance matching and radiation effects that must be considered.

Few attempts have been made to solve this problem. Alexopoulos and Jackson [2] solved the problem of an electric dipole radiating in a substrate–superstrate structure by formulating the Green's function. The basic properties of radiation in such an environment have been discussed in their paper. One significant result in their work was that a superstrate with dielectric constant higher than that of the substrate may, at the proper thickness, reduce to a minimum the surface-wave excitation and increase the radiation efficiency. This result motivated our inquiry and interest into the possibility of increasing the dielectric cover thickness to a maximum (mechanical considerations) without paying a significant price in extra losses due to radiation efficiency decrease (excessive surface-wave excitation).

Bhattacharyya and Tralman [3] have conducted an empirical study of the dielectric superstrate effects on a patch antenna. Bhattacharyya [4] analyzed the radiation properties of a circular patch in a substrate–superstrate structure by implementing the cavity model to solve the problem. Benalla and Gupta [5] have introduced the multiport network model to analyze the radiation from a rectangular microstrip antenna covered with a dielectric layer. In their analysis they considered the special case in which the dielectric constants of the superstrate and substrate are equal. Tu and Chang [6] used the Wiener–Hopf technique to compute the effect of the cover layer on the edge admittance of a semiinfinite microstrip line as an interim step to compute the performance of a covered patch antenna.

In the work reported in this paper the substrate and superstrate can have arbitrary dielectric constants. An improved transmission line model, which accounts for the external mutual coupling between the two equivalent slots of the radiating patch, is used, and a 4×4 microstrip array was designed, built, and tested to validate the analysis. Section II describes the theory of the method. The general Green's function of an elementary magnetic dipole in a superstrate–substrate structure, utilizing spectral domain analysis, is formulated, and the surface-wave and radiation fields are computed. The transmission line model is used to compute the input impedance and the radiation efficiency. Section III compares numerical results to measured results for a single patch and a 4×4 element array.

Manuscript received February 26, 1993; revised October 18, 1993.

The author is with the Department of Electrical Engineering, Ben-Gurion University of the Negev, Beer-Sheva 84105, Israel.

IEEE Log Number 9403668.

II. Theory

A. Green's Function Formulation

The basic geometry of a rectangular microstrip antenna covered by a dielectric layer is shown in Fig. 1. The patch is rectangular with width b and length a. The substrate–superstrate thickness and dielectric constants are d_1, ε_1 and d_2, ε_2, respectively. The substrate used is assumed to be thin so that the fields underneath the patch have no z variations. The patch constitutes a cavity with radiating magnetic walls. By the Schelkunoff equivalence principle the radiation from the cavity magnetic walls can be approximated by two x-directed magnetic current sheets with spacing a, length b, width d_1, and located at a height d_1 above the ground plane. Near resonance of the dominant mode, the patch radiation is due to the fringing fields of the radiating edges at $y = \pm a/2$. For the purposes of the computation of the edge admittances, the fields of an elementary x-directed magnetic dipole located at the interface between the substrate and superstrate layers at (x_0, y_0, d_1) is needed. The x and y components of the electric field in terms of the plane-wave spectrum can be written as

$$E_x(x,y,z) = \frac{1}{4\pi^2} \times \int_{-\infty}^{\infty} \tilde{G}_{xx}(k_x,k_y) e^{jk_x(x-x_0)+jk_y(y-y_0)} dk_x dk_y, \tag{1}$$

$$E_y(x,y,z) = \frac{1}{4\pi^2} \times \int_{-\infty}^{\infty} \tilde{G}_{yx}(k_x,k_y) e^{jk_x(x-x_0)+jk_y(y-y_0)} dk_x dk_y. \tag{2}$$

The transverse field (in x and y directions) and their Fourier transform in all three regions under consideration (substrate, superstrate, and free space above) can be expressed in terms of their z components, E_z, H_z and $\tilde{E}_z$, $\tilde{H}_z$, respectively. The next step would be to impose the boundary conditions in all three regions for the transverse electric and magnetic components. On the ground plane ($z = 0$) the transverse electric fields vanish. At the interface between the substrate and superstrate ($z = d_1$) we impose the continuity of the magnetic fields and the jump condition for the electric fields on an elementary x-directed magnetic dipole. At the interface of the superstrate and free space ($z = d, d = d_1 + d_2$) the transverse electric and magnetic fields are continuous. Proceeding through all these steps we obtain after some algebraic manipulations the fields in all three regions. The z components of the Fourier transform electric and magnetic fields can be written in the form

$$\tilde{E}_z = k_y Q_i(\beta, z) e^{-jk_x x_0 - jk_y y_0}$$
$$\tilde{H}_z = k_x P_i(\beta, z) e^{-jk_x x_0 - jk_y y_0} \qquad i = (1,2,3) \tag{3}$$

in which

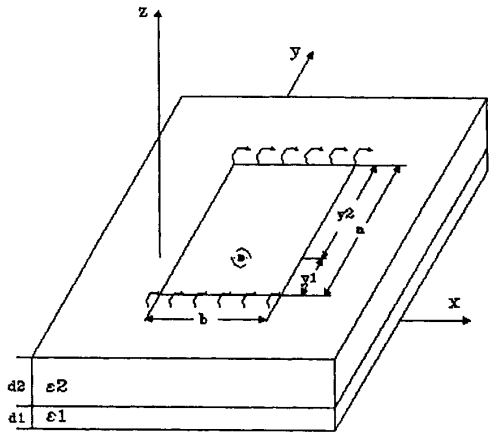

Fig. 1. The geometry of a covered rectangular microstrip antenna.

Region 1: $(0 < z < d_1)$

$$Q_1(\beta, z) = -\frac{j\varepsilon_2(k_2 \cos k_2 d_2 + \gamma_3 \varepsilon_2 \sin k_2 d_2)}{T_m} \cos k_1 z, \tag{4}$$

$$P_1(\beta, z) = \frac{k_2(k_2 \sin k_2 d_2 - \gamma_3 \cos k_2 d_2)}{k_0 \eta_0 T_e} \cos k_1 z, \tag{5}$$

$$k_1 = \sqrt{k_0^2 \varepsilon_1 - \beta^2}; \quad k_2 = \sqrt{k_0^2 \varepsilon_2 - \beta^2};$$

$$\gamma_3 = \sqrt{\beta^2 - k_0^2}; \quad \beta^2 = k_x^2 + k_y^2; \quad \eta_0 = 120\pi, \tag{6}$$

$$T_m = k_1 \varepsilon_2 \sin k_1 d_1 (k_2 \cos k_2 d_2 + \gamma_3 \varepsilon_2 \sin k_2 d_2) + k_2 \varepsilon_1 \cos k_1 d_1 (k_2 \sin k_2 d_2 - \gamma_3 \varepsilon_2 \cos k_2 d_2), \tag{7}$$

$$T_e = k_2 \sin k_1 d_1 (k_2 \sin k_2 d_2 - \gamma_3 \cos k_2 d_2) - k_1 \cos k_1 d_1 (k_2 \cos k_2 d_2 + \gamma_3 \sin k_2 d_2). \tag{8}$$

Region 2: $(d_1 < z < d)$

$$Q_2(\beta, z) = -\frac{j\varepsilon_1 \cos k_1 d_1 \left(k_2 \cos k_2 (d - z) + \gamma_3 \varepsilon_2 \sin k_2 (d - z)\right)}{T_m}, \tag{9}$$

$$P_2(\beta, z) = \frac{k_1 \cos k_1 d_1 \left(k_2 \cos k_2 (d - z) + \gamma_3 \sin k_2 (d - z)\right)}{k_0 \eta_0 T_e}. \tag{10}$$

Region 3: $(z > d)$

$$Q_3(\beta, z) = -\frac{jk_2 \varepsilon_1 \varepsilon_2 \cos k_1 d_1}{T_m} e^{-\gamma_3 (z-d)}, \tag{11}$$

$$P_3(\beta, z) = \frac{k_1 k_2 \cos k_1 d_1}{k_0 \eta_0 T_e} e^{-\gamma_3 (z-d)}. \tag{12}$$

Using (3) we can take the inverse Fourier transform to obtain the real fields

$$E_z = \frac{1}{4\pi^2} \int_{-\infty}^{\infty} \int_{-\infty}^{\infty} k_y Q_i(\beta, z) e^{jk_x(x-x_0) + jk_y(y-y_0)} dk_x dk_y \tag{13}$$

$$H_z = \frac{1}{4\pi^2} \int_{-\infty}^{\infty} \int_{-\infty}^{\infty} k_x P_i(\beta, z) e^{jk_x(x-x_0) + jk_y(y-y_0)} dk_x dk_y.$$

Given the z components of the fields, the transverse components can be computed through Maxwell equations.

B. Surface-Wave Contribution

The poles β_0 of $\tilde{E}_z$ and $\tilde{H}_z$ are determined by the zeros of T_m and T_e and represent the transverse magnetic (TM) and transverse electric (TE) surface-wave poles, respectively. For lossless mediums these poles, β_0, are real and their locations occur in the range $k_0 < \beta_0 < \max(\sqrt{\varepsilon_1} k_0, \sqrt{\varepsilon_2} k_0)$. In this work we have considered only the dominant TM surface-wave mode, since it has the major effect in most applications. However, the same procedure can be applied for higher order modes. Evaluation of E_z in (13) gives the total field, which is composed from the radiated and the surface-wave fields. Analytical evaluation of the integral in (13) requires a change of coordinates to $k_x = \beta \cos \alpha$, $k_y = \beta \sin \alpha$ and $x = \rho \cos \phi$, $y = \rho \sin \phi$. The new integration range is $\beta = 0$ to ∞ and $\alpha = 0$ to 2π. The integration on α can be performed analytically [7] using the integral form of the first-order Bessel function. The integration on β is extended from $-\infty$ to ∞ by replacing the Bessel function with Hankel function, to obtain

$$E_z(\rho, \phi, z) = -j\pi \sin \phi \int_{-\infty}^{\infty} \frac{\beta^2}{4\pi^2} Q(\beta, z) H_1^{(2)}(\beta\rho) d\beta \tag{14}$$

in which $H_1^{(2)}(\beta\rho)$ is the second Hankel function of the first order. The path of integration from $-\infty$ to ∞ can be extended as shown in Fig. 2. The integration path is deformed to avoid crossing the branch cut at $-k_0$ and includes the surface-wave pole at $-\beta_0$. Using the theory of residues the value of the contour integral can be computed by

$$\int_c \frac{f(\beta)}{T_m(\beta)} d\beta = -2\pi j \frac{f(\beta_0)}{T_m'(\beta_0)} \tag{15}$$

where $T_m'(\beta_0)$ is T_m derivative. The integration over the portion of the contour with $|\beta| \to \infty$ vanishes. Thus, the integral given by (14) (the total field) is equal to the integration around the branch cut plus the residue contribution. The integration around the branch cut gives the radiated field, while the residue contribution gives the surface wave field. A simpler way to compute the radiated field is through the steepest descent method as explained in the next section. Evaluation of the RHS of (15) in all three regions gives the surface-wave fields.

$$E_z^{\mathrm{sw}}(\rho, \phi, z) = \frac{\beta_0}{2} \sin \phi U_i(\beta_0, z) H_1^{(2)}(\beta_0 \mid \rho - \rho_0 \mid) \tag{16}$$

where $i = 1, 2, 3$ stand for regions 1, 2, and 3, and U_i is equal to the expressions (4), (9), or (11) in which T_m is replaced by its derivative T_m'.

Integration of E_z^{sw} over each of the patch edges of length b results in the total surface-wave field radiated. Near resonance, the current distribution of the equivalent magnetic current on the edge is constant, an assumption used in the integration over the edge. The fringing fields at the nonradiating edges (of length a) are accounted for by moving the location of the magnetic walls outward by an appropriate amount. The new radiating edge length is denoted by b_{eff} [8]. The surface-wave power radiated by each of the two radiating edges is given by

$$P_{\mathrm{sw}} = \frac{1}{2} \mathrm{Re} \int_0^{\infty} \int_0^{2\pi} E_z^{\mathrm{sw}} H_\phi^{\mathrm{sw}^*} \rho d\phi dz \Big|_{\rho \to \infty}. \tag{17}$$

The integration is performed in all three regions, and the sum of the results yields the total surface wave radiated by each of the two radiating edges. The integration on z can be performed analytically, while the integration over ϕ must be performed numerically. The

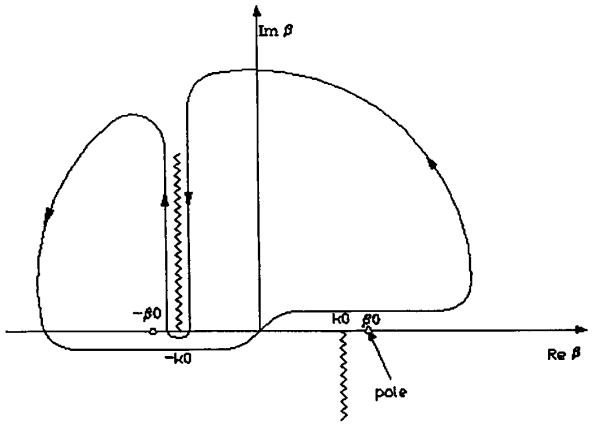

Fig. 2. The integration path contour in β plane.

power coupled to the surface wave can be represented by an edge conductance G_s [5]

$$G_s = \frac{2P_{\text{sw}}}{\frac{1}{b}\int_s V^2(s)ds} \tag{18}$$

where the integration is along the patch edge of length b and $V(s)$ is the voltage distribution along the edge. P_{sw} is the power radiated by the surface wave and is computed in (17). For a rectangular patch operating near resonance of the dominant mode, $V(s)$ is uniform, and in this case (18) simplifies to $G_s = 2P_{\text{sw}}$.

C. Radiation Fields

The radiated fields in region $3(z > d)$ can be computed from (11), (12), and (13) given that $\beta < k_0$ (the visible range). In this instance, γ_3 is replaced by $-jk_3$. The computation of the integral in (13) can be facilitated if we make change of variables to spherical coordinates $x = r\sin\theta\cos\phi$, $y = r\sin\theta\sin\phi$, $z = r\cos\theta$, $k_x = k_0\sin\alpha\cos\delta$, $k_y = k_0\sin\alpha\sin\delta$. Evaluation of the integrals in (13) for $r \to \infty$ and using the steepest descent method gives the field expressions in spherical coordinates

$$E_\theta = j\frac{k_0\varepsilon_1\varepsilon_2 b_{\text{eff}}}{2\pi}\frac{e^{-jk_0r}}{r}\frac{u_2\cos k_0u_1d_1}{T_m} \sin c\left(k_0\frac{b_{\text{eff}}}{2}\sin\theta\cos\phi\right)\cos\theta\sin\phi, \tag{19}$$

$$E_\phi = -j\frac{k_0 b_{\text{eff}}}{2\pi}\frac{e^{-jk_0r}}{r}\frac{u_1u_2\cos k_0u_1d_1}{T_e} \sin c\left(k_0\frac{b_{\text{eff}}}{2}\sin\theta\cos\phi\right)\cos\theta\cos\phi \tag{20}$$

where

$$u_1 = \sqrt{\varepsilon_1 - \sin^2\theta}; \quad u_2 = \sqrt{\varepsilon_2 - \sin^2\theta}, \tag{21}$$

$$\begin{aligned} T_m = {} & u_1\varepsilon_2\sin k_0u_1d_1(u_2\cos k_0u_2d_2 + j\cos\theta\varepsilon_2\sin k_0u_2d_2) \\ & + u_2\varepsilon_1\cos k_0u_1d_1 \\ & \times (u_2\sin k_0u_2d_2 - j\cos\theta\varepsilon_2\cos k_0u_2d_2), \end{aligned} \tag{22}$$

$$\begin{aligned} T_e = {} & u_2\sin k_0u_1d_1(u_2\sin k_0u_2d_2 - j\cos\theta\cos k_0u_2d_2) \\ & - u_1\cos k_0u_1d_1(u_2\cos k_0u_2d_2 + j\cos\theta\sin k_0u_2d_2). \end{aligned} \tag{23}$$

The power radiated by each of the radiating edges can be evaluated by integrating the Poynting vector over the upper hemisphere of the patch.

$$P_r = \frac{1}{2}\text{Re}\int_0^{2\pi}\int_0^{\frac{\pi}{2}}\frac{E_\theta E_\theta^* + E_\phi E_\phi^*}{\eta_0}r^2\sin\theta d\theta d\phi. \tag{24}$$

The equivalent conductance of each radiating edge is G_r and can be computed by (18), in which P_{sw} is replaced by P_r to give $G_r = 2P_r$. This result is obtained based on the assumption that the distribution of the dominant mode voltage $V(s)$ over the radiating edge is uniform. The double integration in (24) is carried out numerically using Gaussian quadrature [7]. The radiation efficiency η_s of the covered patch antenna is the ratio of the radiated power P_r to the total (radiated plus surface-wave) power.

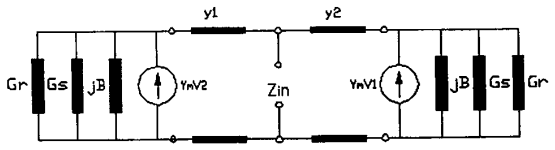

Fig. 3. The equivalent transmission line circuit of the loaded rectangular microstrip antenna.

D. Impedance Model

The transmission line model to analyze rectangular uncovered patch antennas was introduced by Munson [1] and improved by Derneryd [9] and Pues *et al.* [10] to consider the stored energy near the edges and the external mutual coupling between the radiating edges. In the present work this model was adopted for the covered patch case. The equivalent circuit of the covered rectangular patch is shown in Fig. 3. G_r and G_s represent the surface-wave and radiation conductances of the radiating edges. The susceptance B represents the stored energy near the edges, and the mutual admittance Y_m represents the external mutual coupling between the two radiating edges. The equivalent transmission line connecting the two edges has a length a, and the feed distance from one of the edges is y_1. The parameters of a covered microstrip line have been computed by Bahl and Stuchly [11] and used in the present work. The characteristic impedance Z_0, the propagation constant β_0, and the effective dielectric constant $\varepsilon_{\text{ra}}(b)$ of a covered microstripline of width b are given by [11].

The edge susceptance B can be expressed in terms of the edge capacitance $C(b)$ by $B = j\omega C(b)$. An approximate method for the computation of the edge capacitance is based on the evaluation of the edge capacitance of a covered microstripline with width a and derived by Wolff and Knoppik [12]:

$$C(b) = \frac{b}{2}\left(\frac{\varepsilon_{\text{ra}}(a)}{v_0 Z_0(\text{air})} - \varepsilon_0\varepsilon_1\frac{a}{d_1}\right) \tag{25}$$

where $\varepsilon_{\text{ra}}(a)$ and $Z_0(\text{air})$ are computed in [11]. The open-end effect of the radiating edge is represented by the susceptance B and can be expressed by an open-end extension Δl of the covered microstripline. Given the expressions, of the fields derived by the spectral-domain analysis (13), the external mutual conductance Y_m can be computed. Alternatively, we can use the expression derived by Pues and Van De Capelle [10], which gives the external conductance Y_m between two radiating edges

$$Y_m = (G_s + G_r)F_g + jBF_bK_b. \tag{26}$$

The parameters F_g, F_b, and K_b can be found in [10]. Given all the circuit parameters as shown in Fig. 3, one can compute the input admittance Y_{in} [10] as shown in (27) at the bottom of the page, where $Y_l = G_r + G_s + jB$ and $Y_0 = 1/Z_0$. A coaxial probe feed can be

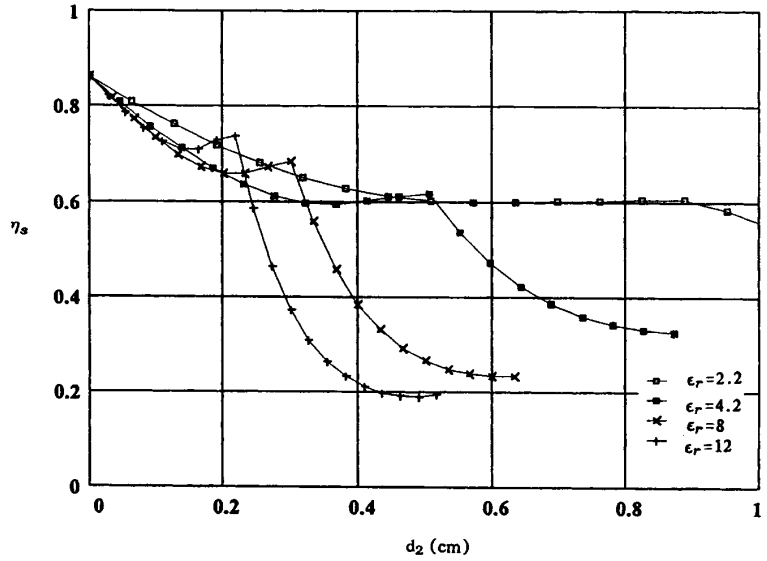

Fig. 4. Radiation efficiency η_s versus superstrate thickness d_2 for various dielectric constants ε_2.

modeled by a coaxial stub in a parallel waveguide [13]. The formula for the probe input impedance Z_f is

$$Z_f = \frac{Z_0}{4} k_0 d_1 \left(1 - j\frac{2}{\pi} \ln \frac{\gamma k_0 \sqrt{\varepsilon_1} r}{2}\right) \tag{28}$$

where $Z_0 = 120\pi$, $\gamma = 1.781$ and r is the probe radius.

III. Results

In this section numerical and measured results will be presented to validate the theory developed in Section II.

Fig. 4 shows the dependence of the radiation efficiency η_s on the superstrate thickness d_2 for various dielectric constants ε_2. The patch dimensions are $a = 1.2$ cm, $b = 1.6$ cm, $d_1 = 0.1575$ cm, $\varepsilon_1 = 2.2$, $\tan\delta_1 = 0.001$, $\tan\delta_2 = 0.0007$, and frequency is 6.4 GHz. One can observe that the efficiency drops monotonically with the increase in the superstrate thickness up to a breaking point, with the approximate value of $d_2 = 0.2\lambda_0/\sqrt{\varepsilon_2}$. Beyond this point a significant drop in the efficiency occurs. In the vicinity of the breaking point, we obtain a local increase in the radiation efficiency due to a local increase in the radiated power P_r. These results confirm those reported in [2]. This phenomenon is especially accentuated for high ε_2. Fig. 4 indicates that lower ε_2 and d_2 should be favored to minimize the decrease in the antenna efficiency. However, there are cases in which materials with low ε_2 and d_2 don't fulfill the mechanical requirements from the cover. In these cases Fig. 4 suggests upper bounds (the breaking points) on ε_2 and d_2 with relatively affordable losses due to the surface-wave excitation. Beyond these upper bounds the decrease in the antenna efficiency is significant.

The increase in ε_2 results in a decrease in the resonance frequency, the impedance of the patch, and the characteristic impedance of the feeding microstrip lines. The decrease in the characteristic impedance of the feeding lines results in an increase in the radiation loss of the network [14]. To restore the characteristic impedance level of the network to that of the uncovered case, the size of the feeding lines must be reduced. In some cases production considerations limit the minimum width of the microstrip lines and extra losses should be expected in the covered case beyond those outlined in the previous paragraph. Moreover, to minimize the dielectric loss of the feeding network low-loss superstrate and substrate materials are required.

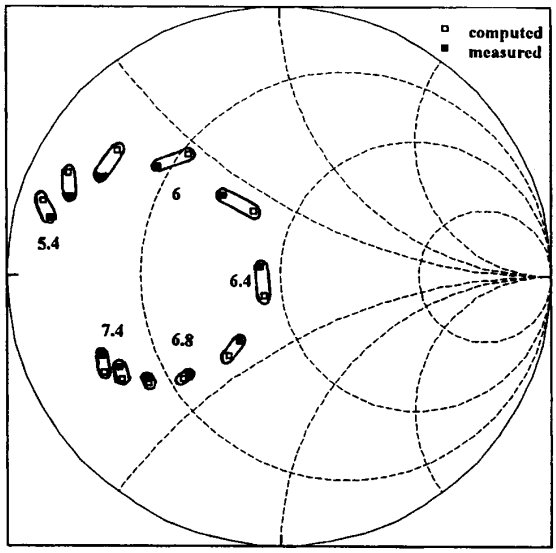

Fig. 5. Comparison between computed and measured data of the input impedance of a single patch ($a = 1.2$ cm, $b = 1.6$ cm, $\varepsilon_1 = 2.2$, $\varepsilon_2 = 4.2$, $d_1 = 0.1575$ cm, $d_2 = 0.21$ cm).

$$Y_{\text{in}} = 2Y_0 \frac{(Y_0^2 + Y_l^2 - Y_m^2) + j2Y_0(Y_m csc(\beta_0 a) - Y_l \cot(\beta_0 a))}{2Y_0 Y_l - j((Y_0^2 + Y_l^2 - Y_m^2)\cot(\beta_0 a) + (Y_0^2 - Y_l^2 - Y_m^2)\cos(\beta_0(y_2 - y_1))csc(\beta_0 a))} \tag{27}$$

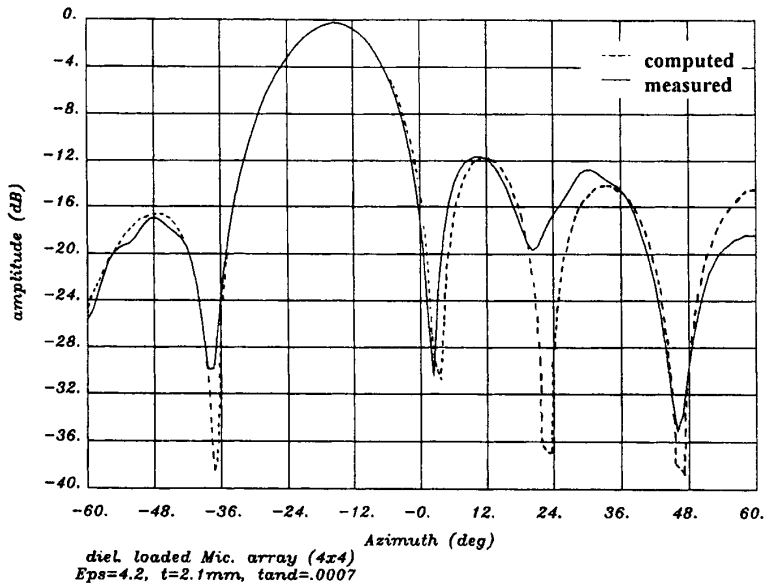

Fig. 6. H-plane radiation pattern of 4 × 4 microstrip array at 6.4 GHz.

As a consequence of these considerations we chose to cover the patch with $\varepsilon_2 = 4.2$ and $\tan\delta_2 = 0.0007$. The superstrate thickness was 0.21 cm. Fig. 5 shows a comparison of the measured and computed values of the patch input impedance for a feeding distance $y_1 = 0.28$ cm (see Fig. 1). The patch was fed coaxially. The computed resonance of the patch was 6.37 GHz, and the measured value was 6.4 GHz. As discussed previously, the dielectric cover decreases the resonance frequency, the resonance impedance, and to some extent the radiation efficiency. Based on the results obtained for a single patch, an array of 4 × 4 elements with a squinted beam (15°) in the H plane was designed and built. The spacing among the elements was $d_x = 0.75\lambda_0$ and $d_y = 0.84\lambda_0$. The feeding network was corporate, and the characteristic impedance of the loaded lines was computed based on [11]. The radiation pattern was measured in a planar near field range. Fig. 6 shows a comparison between the computed and measured H-plane patterns of the array at the resonance frequency 6.4 GHz. One can observe a good agreement between the two. The directivity of the array was 20.4 dBi, while the measured gain was 19 dBi. An equivalent uncovered array has a gain of 20 dBi, and the difference of 1 dB can be attributed to the difference in the efficiencies, 85% in the uncovered case and 65% for the covered case. An attempt was made to cover the array with a dielectric sheet of the same dimensions and ε_2, but with a higher loss tangent, $\tan\delta_2 = 0.0245$, this resulted in an additional loss of 1 dB due to the extra loss of the feeding structure. Consequently, low-loss materials for the cover or, alternatively, separation of the feeding network from the radiating elements, a technique discussed in [15], must be used to insure high radiation efficiency.

IV. Conclusion

This paper presents the analysis of a rectangular microstrip antenna covered with an arbitrary dielectric layer. In the analysis, the Green's function of an elementary magnetic dipole is evaluated and the transmission line model is used to compute the input impedance. Numerical results on the effect of the dominant TM surface wave excited and its impact on the radiation efficiency and input impedance are presented. A single patch and a 4 × 4 microstrip array were built. The theoretical and measured results are in good agreement.

References

[1] R. Munson, "Conformal microstrip antennas and microstrip phased arrays," *IEEE Trans. Antennas Propagat.*, vol. AP-22, pp. 74–78, 1974.
[2] N. G. Alexopoulos and D. R. Jackson, "Fundamental superstrate (cover) effects on printed circuit antennas," *IEEE Trans. Antennas Propagat.*, vol. AP-32, pp. 807–816, 1984.
[3] A. K. Bhattacharyya and T. Tralman, "Effects of dielectric superstrate on patch antennas," *Electron. Lett.*, vol. 24, pp. 356–358, 1988.
[4] A. K. Bhattacharyya, "Characteristics of circular patch on thick substrate and superstrate," *IEEE Trans. Antennas Propagat.*, vol. 39, pp. 1038–1041, 1991.
[5] A. Benalla and K. C. Gupta, "Multiport network model for rectangular microstrip patches covered with a dielectric layer," *IEE Proc.*, vol. 137, pp. 377–383, 1990.
[6] Y. Tu and D. C. Chang, "Effect of a cover layer on the edge admittance of a wide microstrip," *IEEE Trans. Antennas Propagat.*, vol. 39, pp. 354–358, 1991.
[7] M. Abramowitz and I. A. Stegun, *Handbook of Mathematical Functions*. New York: Dover, 1972, pp. 360–361.
[8] I. J. Bahl and P. Bhartia, *Microstrip Antennas*. Norwood, MA: Artech, 1980, ch. 2.
[9] A. G. Derneryd, "A theoretical investigation of the rectangular microstrip antenna element," *IEEE Trans. Antennas Propagat.*, vol. AP-26, pp. 532–535, 1978.
[10] H. Pues and A. Van de Capelle, "Accurate transmission-line model for the rectangular microstrip antenna," *IEE Proc.*, vol. 131H, pp. 334–340, 1984.
[11] I. J. Bahl and S. S. Stuchly, "Analysis of a microstrip covered with a lossy dielectric," *IEEE Trans. Microwave Theory Tech.*, vol. MTT-28, pp. 104–109, 1980.
[12] I. Wolff and N. Knoppik, "Rectangular and circular microstrip disk capacitors and resonators," *IEEE Trans. Microwave Theory Tech.*, vol. MTT-22, pp. 857–864, 1974.
[13] R. F. Harrington, *Time-Harmonic Electromagnetic Fields*. New York: McGraw-Hill, 1961, p. 378.
[14] E. Levine, G. Malamud, S. Shtrikman, and D. Traves, "A study of microstrip array antennas with the feed network," *IEEE Trans. Antennas Propagat.*, vol. 37, pp. 426–434, 1989.
[15] D. M. Pozar, "A reciprocity method of analysis for printed slot and slot-coupled microstrip antennas," *IEEE Trans. Antennas Propagat.*, vol. AP-34, pp. 1439–1446, 1986.